Quantitatively Differentiating Antibodies Using Charge-State Manipulation, Collisional Activation, and Ion Mobility – Mass Spectrometry

Activation, and fon Modifity – Mass Spectrometry
Theresa A. Gozzo, Matthew F. Bush*
Contribution from:
Department of Chemistry
University of Washington
Box 351700
Seattle WA 98195-1700
Address correspondence to: <u>mattbush@uw.edu</u>

Abstract

Antibody-based therapeutics continue to expand both in the number of products and their use in patients. These heterogeneous proteins challenge traditional drug characterization strategies, but ion mobility (IM) – mass spectrometry (MS) approaches have eased the challenge of higher-order structural characterization. Energy-dependent IM-MS, e.g., collision-induced unfolding (CIU), has been demonstrated to be sensitive to subtle differences in structure. In the present study, we combine a charge-reduction method, cation-to-anion proton-transfer reactions (CAPTR), with energy-dependent IM-MS and varied solution conditions to probe their combined effects on the gas-phase structures of IgG1κ and IgG4κ from human myeloma. CAPTR paired with MS-only analysis improves the confidence of charge-state assignments and the resolution of interfering protein species. Collision cross-section distributions were determined for each of the charge-reduced products. Similarity scoring was used to quantitively compare distributions determined from matched experiments analyzing samples of the two antibodies. Relative to workflows using energy-dependent IM-MS without charge-state manipulation, combining CAPTR and energy-dependent IM-MS enhanced the differentiation of these antibodies. Combined, these results indicate that CAPTR can benefit many aspects of antibody characterization and differentiation.

Introduction

Monoclonal antibodies (mAbs) constituted 4 out of 10 of the top drugs by sales in 2021¹ and the list of approved mAbs therapeutics continues to expand.² All currently approved mAb therapeutics are based on Immunoglobulin Gammas (IgGs).^{3,4} Relative to small-molecule therapeutics, mAbs have resisted general strategies for characterization and quality control. They are large, flexible molecules rich with post-translational modifications, making them heterogeneous. 5,6 These properties challenge high-resolution structural techniques and only a few atomic-resolution structures for full-length, intact antibodies have been reported.^{7–9} These challenges have motivated the use of complementary techniques. ¹⁰ Ion mobility (IM) mass spectrometry (MS) is fast, sensitive, and tolerant of heterogeneity and dynamics. In IM, ions are separated by size, shape, and charge by collisions with background gas molecules in the presence of an electric field; their mobilities can be used to determine what is commonly referred to as a collision cross-section (Ω). This can be used in conjunction with native MS, which provides information about the mass and noncovalent interactions of analytes. Protein ions generated by electrospray ionization (ESI) from native-like solution conditions can have similar Ω values to those predicted based on condensed-phase structures, consistent with the retention of aspects of native structure in the gas phase. 11,12 Complementary methods have corroborated these conclusions, e.g., GroEL ions were soft-landed following MS, and the resulting electronmicroscopy images were consistent with the retention of solution-phase structures. 13,14

IM-MS has been used to characterize multispecific antibodies,¹⁵ differentiate disulfide variants,^{16,17} glycosylation variants,¹⁸ and IgG subclasses,¹⁶ measure the drug-to-antibody ratios of antibody-drug conjugates,^{19,20} and more. The subjects of the present study, IgG1 and IgG4, share more than 90% sequence identity, and they differ not in terms of number, but in

connectivity of their disulfide bonds.⁴ The apparent Ω distributions for IgG1 and IgG4 have been reported to be similar to each other, ^{21,22} but centered at Ω values that are more than 30% smaller than those calculated for the few existing crystal structures of IgGs.^{21–24} Furthermore, the apparent Ω distributions are wider than those for other protein complexes of similar masses.^{21,22} The small magnitude and large widths of the apparent Ω distributions have been attributed to the flexibility of IgGs in solution, specifically that of the hinge region, ²¹ and the structural collapse upon entry into the gas phase.^{21–24} Collision-induced unfolding (CIU) has been demonstrated to be sensitive to subtle differences in gas-phase IgG structures. In CIU, ions are subjected to increasing collisional activation, their arrival times are monitored via IM, and the resulting unfolding patterns can be used to distinguish ion populations. Although IgG1 and IgG4 are difficult to differentiate based on IM-MS measurements alone, they do show distinct unfolding patterns with CIU.^{16,25}

The charge states of gas-phase protein ions depend on the size and structure of the protein, the properties of the solvent and other solutes, the ionization mechanism, and other factors. $^{26-29}$ Charge-state manipulation of protein ions can help probe the effects of charge on the properties of those ions. 30 Several charge-reduction methods have been implemented with MS, $^{31-34}$ and with IM, it is also possible to probe structural changes in relation to charge state. Building upon the pioneering contributions of McLuckey and coworkers, 35 we introduced Cation-to-Anion Proton-Transfer Reactions (CAPTR) to generate a series of charge-reduced protein ions that can be analyzed in parallel. 33 For example, we used CAPTR to investigate the effects of charge state, solution conditions, and internal disulfide bonding on Ω for a large, multidomain protein, bovine serum albumin (BSA). 28 Ions generated from denaturing conditions exhibited Ω values that depended strongly on z, whereas ions from native-like conditions depended weakly

on z. The CAPTR products of single domain proteins from denaturing conditions and native-like ions of the same charge states can exhibit similar Ω values, 36,37 but the lowest-z CAPTR products of BSA from denaturing conditions exhibited Ω values that were significantly larger those for the corresponding native-like ions.²⁸ CAPTR results for BSA²⁸ and lysozyme³⁷ from denaturing, disulfide-reducing conditions indicate that those ions compact more per CAPTR event than the corresponding ions from disulfide-intact conditions. These results suggest that disulfide bonds limit expansion to larger Ω at high z, but also limit compaction at low z. Collisional activation in combination with CAPTR, i.e., pre- or post-CAPTR activation, has aided in differentiating ions with similar apparent Ω distributions. For example, Ω distributions of 8+ ubiquitin appeared to be independent of applied activation voltage, but Ω distributions of 6+ ions generated by CAPTR of the activated 8+ precursors depended on the extent of activation; these differences provided indirect evidence for unresolved, energy-dependent structural changes in the precursor.³⁸ Additional results from CAPTR-based experiments and comparisons with results from other charge-reduction methods have been reviewed recently.³⁰ Overall, these results support the ideas that solution conditions and disulfide bonding impact gas-phase protein ion structure and suggest that charge should be considered when using IM-MS to study biomolecular structure.

Based on CIU of IgGs, ^{16,25} CAPTR of BSA, ²⁸ and pre-CAPTR activation of ubiquitin, ³⁸ we hypothesized that combining charge-state manipulation and energy-dependent IM may enable better differentiation of antibodies than either technique alone. Here, we tested that hypothesis using a combination of experiments and quantitative comparisons of results for IgG1 and IgG4 using similarity scoring³⁹ implemented with the Jensen-Shannon distance metric. ^{40–42}

Methods

Samples. Samples of IgG1κ and IgG4κ (product/lot numbers: I5154/SLCB8124 and I4639/SLBR4231V, respectively) from human myeloma plasma were purchased from Sigma-Aldrich (St. Louis, MO). For native-like conditions, 20 μL samples with a concentration of 1 mg mL⁻¹ (~7 μM) antibody were exchanged into aqueous 200 mM ammonium acetate at pH 7.0 using Micro Bio-Spin 6 columns (Bio-Rad, Hercules, CA). For denaturing conditions, the same procedure was used, but the samples were instead exchanged into aqueous 0.1% acetic acid.

Experiments. All experiments were conducted on a Waters Synapt G2 HDMS modified with a glow-discharge ionization source⁴³ and a radio-frequency confining drift cell (Figure 1a). 44 Cations were generated using electrokinetic electrospray ionization, as described previously. 45 The sample capillary was inserted into a copper block that was maintained at 25 °C using a Peltier device. The atmospheric-pressure interface was maintained at 120 °C for the duration of CAPTR experiments to reduce fouling of the source and ion optics; the temperature of the sample capillary and atmospheric-pressure interface are independent in these experiments.³⁶ To perform CAPTR, perfluoro-1,3-dimethylcyclohexane (PDCH, Sigma-Aldrich, St. Louis, MO) was introduced as a vapor in nitrogen gas. After glow-discharge ionization, the fragments, the monoanion [PDCH-F]⁻ at m/z 381, were quadrupole selected and accumulated in the trap for 100 ms. The instrument polarity was then switched to positive mode to allow selected cations of IgG1 or IgG4 to be transmitted through the trap cell of accumulated anions for 1 to 5 s.³³ Product ions and residual precursor ions were then pulsed into the mobility cell for 200 µs every 36.4 ms. The sampling cone voltage was varied between 25 and 125 V to probe the effects of pre-CAPTR activation, and the trap bias was varied between 5 and 100 V to probe the effects of post-CAPTR activation (Figure 1b). For collision-induced unfolding (CIU)

experiments without CAPTR, cations of a single charge state were selected, and the trap collision voltage was ramped from 5 to 200 V (Figure 1b). For most experiments, IM arrival-time distributions were measured using an RF-confining drift cell⁴⁴ filled with approximately 1.5 Torr helium for most experiments. For post-CAPTR activation experiments, 0.9 Torr nitrogen drift gas was used instead. Additional details of the IM experiments and calculating collision cross sections (Ω) are described in the Supporting Information.

Results and Discussion

The goal of this study was to probe the relationship between solution conditions, charge state, and Ω for highly flexible macromolecules and to determine whether their responses to activation could be used to rapidly differentiate similar proteins. To achieve this goal, we characterized the gas-phase structures of IgG1 κ and IgG4 κ from human myeloma, which will be referred to as IgG1 and IgG4, using CAPTR and IM-MS as a function of solution conditions and energy. Ions originating from electrospray of two different solution conditions were analyzed by MS and IM-MS experiments. Selected ions were subjected to CAPTR to probe the relationship between charge and Ω . And finally, results from collisional activation in combination with CAPTR were used to compare IgG1 and IgG4 ion stabilities and structures.

Differentiation of IgGs by Charge State Assignment and Mass Determination. Figures 2a-d show the mass spectra of IgG1 and IgG4 from native-like conditions of samples held at 25 °C; similar mass spectra were also obtained without temperature control of the sample (Figure S1). Ions generated from native-like conditions will be denoted with a superscript "N", e.g., ^NIgG1. Like other large proteins, the mass spectra of ^NIgG1 and ^NIgG4 display a narrow charge-state distribution with high *m/z* values. The degree of similarity between these spectra should also be

noted; it is challenging to distinguish IgG1 and IgG4 from these results alone. Simulated mass spectra are overlayed on top of the experimental native mass spectra based on the charge-state assignment of the peaks at 6195 m/z (N IgG1) and 6227 m/z (N IgG4) as either 24+ or 25+; the simulated native mass spectra agree reasonably well with the experimental native mass spectra for both sets of charge-state assignments.

The ions near $6200 \, m/z$ were also quadrupole-isolated and subjected to CAPTR; the experimental CAPTR spectra are shown in Figure 2e-h. CAPTR mass spectra were also simulated based on the masses determined from the 24+ and 25+ models of the native mass spectra. The experimental and simulated CAPTR spectra agree only when the peaks near 6200 m/z are assigned to 24+ for NIgG1 and 25+ for NIgG4. Some mass spectra of NIgG1 and NIgG4 from the same source have been assigned so that peaks with similar m/z for both proteins have the same charge state. 16,21 For the IgG samples used in this investigation, the additional peaks generated by CAPTR reveal that these two analytes have different charge-state distributions and different masses. Figures S2 and S3 show the standard deviations associated with propagating mass through various charge-state assignments of the precursor and charge-reduced ion peaks. The analysis resulted in average masses of $148,714 \pm 58$ Da and $155,826 \pm 61$ Da (95%) confidence interval) for IgG1 and IgG4, respectively, under these minimally activating conditions. This analysis suggests that previously reported charge-state assignments for this N IgG4 κ sample may be incorrect. 16 Different post-translational modifications on IgG1 and IgG4 may contribute to the observed mass difference between these two samples. IgG glycosylation can represent 2% to 3% of the total antibody molecular weight. 3,46 With minimal applied activation, incomplete desolvation could contribute to the overall masses as well, but this likely affected both analytes similarly. With increased collisional activation in the source (up to 125 V

sampling cone voltage), the mass difference decreased to 6.7 kDa from 7.1 kDa. Regardless, this analysis highlights the potential ambiguity in interpreting native mass spectra of high mass ions and showcases the application of CAPTR to increase the confidence in native MS charge-state and mass assignments.³³ In this case, despite exhibiting similar native mass spectra, CAPTR also enabled the rapid differentiation of NIgG1 and NIgG4 ions by mass alone.

IgG1 and IgG4 ions generated from aqueous 0.1% acetic acid display a much wider charge-state distribution and higher charge states overall than those from native-like conditions. Ions generated from these denaturing conditions will be denoted with a superscript "D", e.g., DIgG1. Figures S5 and S6 show mass spectra of DIgG1 and DIgG4 from ESI. The highest resolved charge states observed for DIgG1 and DIgG4 were 50+ and 58+, respectively. The lowest charge state observed for both DIgG1 and DIgG4 was 27+. Bimodal charge-state distributions were observed for each sample: one at lower *m/z* and one at higher *m/z*. The presence of higher *m/z* distributions, like those observed for NIgG1 and NIgG4, suggest that these conditions were only partially denaturing, but will be referred to as denaturing for simplicity.

Precursor ions (P) of ^DIgG1 and ^DIgG4 were also subjected to CAPTR prior to mass analysis. When CAPTR was performed on either all ions (no precursor selection), P = 47 or 49 for ^DIgG1, or P = 49 for ^DIgG4, a single series of products were generated (Figures S5 to S10). The masses of these products are consistent with the analysis of native-like ions discussed above. Interestingly, when CAPTR was performed on P = 47 for ^DIgG4, two series of product ions were generated that have masses 155.6 kDa and 158.9 kDa (Figure S5). These species were unresolved in the spectra of both the full population of ESI-generated ions and the CAPTR products of that full population (S8). The 155.6 kDa species is predominant in this spectrum, consistent with the other spectra of this sample (Figures S5 to S10) and that form being

predominant in solution. No evidence for a 3.3 kDa fragment ion was observed, consistent with the presence of the 155.6 kDa species in solution and the absence of fragmentation in CAPTR experiments.³⁰ These two species represent different antibody proteoforms in the original sample, and may differ in sequence, glycosylation, and other properties. Resolving interfering populations is another benefit of CAPTR that could aid in the analysis of challenging biopharmaceutical samples.

Collision Cross-Section (Ω) Values and Solution Conditions. Ω with helium ($^{DT}\Omega_{He}$) were determined from field-dependent measurements of drift time as a function of reciprocal drift voltage. Arrival-time distributions were found to be unimodal for electrospray-generated ^NIgG ions. The centroid of each distribution was estimated from that of the best-fit normal distribution, as described previously. 47 Figure S4 shows CCS values calculated based on different chargestate assignments. When the charge states are assigned based on the CAPTR mass spectra, the ^{DT}Ω_{He} values of the ^NIgG1 and ^NIgG4 ions differ by less than 2%. The 24+ and 23+ populations are most similar in size with a <0.6% difference. With such small differences in Ω , IgG1 and IgG4 cannot be differentiated by Ω alone. Within samples, the Ω values ranged from 67.6 to 69.6 nm² (3% difference) for 22+ to 27+ IgG1 and 67.9 to 72.1 nm² (6% difference) for 23+ to 28+ IgG4. For comparison, 24+ to 27+ alcohol dehydrogenase (mass of 147 kDa) exhibited ^{DT}Ω_{He} that differed by up to 3.5%. 48 If IgG1 and IgG4 are assumed to have more similar masses, i.e., peaks at similar m/z in both spectra are both incorrectly assigned the same charge state (Figure 2), the apparent maximum difference in Ω grows to 3.9% for the 22+ or 23+ populations, depending on the misassignment (Figure S4). These results illustrate how charge-state assignment can impact the interpretation of ion mobility results.

The $^{DT}\Omega_{He}$ values for ions from denaturing conditions ranged from 69.2 to 112.2 nm² (47% difference) for $^{D}IgG1$ and 72.6 to 132.0 nm² (58% difference) for $^{D}IgG4$. For comparison to $^{D}IgG1$, 50+ ions of $^{D}IgG4$ had a Ω value of 114.0 nm². Ions of charge states also observed under native-like conditions exhibited similar centroid Ω values to their native-like counterparts (Figure S10). Relative to $^{N}IgG1$ and $^{N}IgG4$ ions, Ω values depended more strongly on charge state, which is consistent with results for other protein ions generated from denaturing conditions. ^{28,36,37} For most charge states, larger differences in Ω values were observed between $^{D}IgG1$ and $^{D}IgG4$ ions than for $^{N}IgG1$ and $^{N}IgG4$. The largest difference was observed for the 31+ charge state (7.8%).

Relationship Between Charge and Ω . Three ^NIgG1 and ^NIgG4 precursors, 26+, 25+, and 24+, and two ^DIgG1 and ^DIgG4 precursors, 49+ and 47+, were selected for analysis based on their intensities and subjected to CAPTR. The CAPTR products originating from each of the precursors were characterized by IM-MS. Arrival-time distributions were converted to median collision-cross sections ($^{DT}\tilde{\Omega}_{He}$) with helium as described in the Supporting Information. Ions are identified by "Condition" where "P" is the charge state of the precursor ion, "C" is the charge state of the CAPTR product, and "Condition" is the solution conditions ("N" or "D"). For the $^{N}P\rightarrow C$ ions, the $\tilde{\Omega}$ values depended weakly on both P and C (Figure 3). Although there were small, systematic differences between the $\tilde{\Omega}$ values of IgG1 and IgG4, but those differences were comparable in magnitude to those for the precursor ions that were not subjected to CAPTR. The Supporting Information includes a more detailed discussion of these values. Compared to other native-like proteins of similar mass, N IgG1 and N IgG4 undergo slightly less compaction with charge reduction, which may be the result of the compaction these molecules have undergone upon entrance into the gas phase, consistent with previous work. $^{23-26}$ The small magnitude of

these differences in Ω are consistent with those for the CAPTR products of other large, native-like protein ions, ^{28,48} as shown for ^NBSA in Figure 3. Overall, the results of these experiments suggest that the excess positive charges on these native-like antibody ions have a small effect on their structures as monitored by CAPTR and IM, which is consistent with our observations for large, well-folded proteins. ^{28,48}

Pre-CAPTR Activation of Ions from Native-Like Conditions. To investigate the relationship between the structures of the precursors and their CAPTR products, ^NIgG ions were analyzed as a function of sampling cone voltage (Figure 1b). Increasing this voltage increases the extent of collisional activation in the atmospheric-pressure interface, which occurs prior to quadrupole selection and CAPTR. Note that collision activation can also result in the loss of

charge,⁴⁹ which may also contribute to these results. An asterisk is used to indicate the activated species, i.e., " $^{N}P^{*}\rightarrow C$." The 26+ and 25+ precursor ions of IgG1 and IgG4 were selected for these experiments and were probed at sampling cone voltages of 25, 50, 75, 100, and 125 V.

Generally, with increasing sampling cone voltage, the apparent $^{DT}\Omega_{He}$ distributions for all observed $^{N}P^{*}\rightarrow C$ ions tended to shift to larger values, increase in width, and exhibit more multimodal character. Figure 4 illustrates these trends for the $^{N}25^{*}\rightarrow C$ ions of IgG1 and IgG4. With decreasing C, the apparent Ω distributions tended to shift to smaller values, decrease in width, and exhibit more unimodal character. These trends are generally consistent with results from pre-CAPTR activation of other native-like ions of proteins. For a given C and sampling cone voltage, the apparent Ω distributions for IgG1 and IgG4 exhibited varying extents of overlap. The extent of that overlap was greatest for the two highest sampling cone voltages. For example, with a sampling cone voltage of 100 V, the distributions for IgG1 and IgG4 exhibited significant overlap and the extent of overlap depended weakly on C. By comparison, with a sampling cone voltage of 75 V, there were greater differences between the distributions for IgG1 and IgG4, and those differences increased with the number of CAPTR events. These results all indicate that the apparent Ω distributions of these antibody ions can depend on the pre-CAPTR activation voltage, C, and the identity of the antibody.

Next, we quantified these differences using similarity scoring. We previously introduced the use of similarity scores to quantify the differences between arrival-time distributions and evaluate the significance of those differences relative to the variance of the underlying measurements.³⁹ Here, we calculated the Jensen-Shannon distance metric, which scores the difference between two probability distributions^{40–42} and has been applied across many fields, including bioinformatics, machine learning, and linguistics.^{50–52} We define the similarity as 1

minus the Jensen-Shannon distance, which is the square root of the Jensen-Shannon divergence.

A more detailed description of this similarity score metric and how it was calculated is available in the Supporting Information.

Figure 4 helps identify the most dissimilar Ω distributions for ^NIgG1 and ^NIgG4 ions formed from 25+* precursors. The apparent Ω distributions at 75 V and 100 V pre-CAPTR activation are shown as examples, and similarity scores comparing Ω distributions at all pre-CAPTR activation voltages are plotted. At most levels of pre-CAPTR activation, the Ω distributions of charge-reduced products exhibit less similarity than the corresponding precursors. For example, using 75 V, the Ω distributions of the 25+* precursor of NIgG1 and N IgG4 yield a similarity score of 0.81, whereas that for the N 25* \rightarrow 12 ions is 0.53. For reference, scores comparing replicates of $^{\rm N}25 \rightarrow C$ at 25 V are all 0.87 or higher (Ω distributions of replicates shown in Figures S11 and S12). Therefore, the low similarity determined for the $^{N}25*\rightarrow 12$ ions from the two samples provides unambiguous evidence that the samples are different, at a higher level of confidence than possible for the 25+* ions from those samples. ^NIgG1 and ^NIgG4 activated precursors display similar Ω distributions, but their 12+ products are extremely sensitive to their differences. Similar trends in similarity scores are seen for ^N26*→C Ω , as shown in Figures S13 and S14. These results provide further evidence that ions with similar Ω values don't necessarily have similar structures.

Collisional activation without charge-state manipulation, i.e., CIU, has been used applied previously to differentiate N IgG1 and N IgG4 from the same source. 16 To directly compare CIU with pre-CAPTR activation, 25+ and 26+ ions of both antibodies were probed as a function of collision energy using methods as indicated in Figure 1b. Figures S16 and S17 show representative Ω distributions. Figure 5 shows the similarity score between the distributions

obtained for each charge state as a function of the collision voltages. The lowest similarity score calculated for ${}^{\rm N}{\rm IgG1}$ and ${}^{\rm N}{\rm IgG4}$ Ω distributions is 0.66, which was for the 26+ ions that were analyzed using a 70 V trap injection voltage with a value of 0.66. This aligns well with the low collision voltage range in which large CIU differences were observed previously for 23+ ions of ${\rm IgG1}\kappa$ and ${\rm IgG4}\kappa$. For comparison, the similarity scores for ${}^{\rm N}{\rm 25}^*{\to}C$ and ${}^{\rm N}{\rm 26}^*{\to}C$ ions at 50 V pre-CAPTR activation are plotted as a function of C. The lowest score achieved from pre-CAPTR activation experiments is 0.41, which was for the 25* \to 13 ions. The apparent Ω distributions resulting from pre-CAPTR activation of the two samples are less similar, i.e., the two samples are better differentiated by pre-CAPTR activation than CIU.

Note that we previously compared Ω distributions using a similarity score that depended on dot products. Analyzing the current results using either that similarity score or the Jensen-Shannon similarity score results in similar trends and identical conclusions (Figure S15). However, in other ongoing projects involving different types of distributions, we identified edge cases for which the dot-product-based similarity score yields values greater than the expected bounds from zero to one. These edge cases were associated with pairs of distributions containing high probabilities for the same values, but for which the dot product of each distribution with itself yields very different values. Based on that finding, we now recommend using the Jensen-Shannon similarity score for comparing distributions from IM experiments.

Post-CAPTR Activation of Ions from Native-Like Conditions. To further probe the gasphase structures of N IgG ions and their CAPTR products, those ions were analyzed as a function of the injection voltage into a nitrogen-filled mobility cell (Figure 1b). This will be referred to as post-CAPTR activation and the activated species are noted with an asterisk, i.e., ${}^{N}P \rightarrow C^{*}$." Only the 26+ precursor ions of IgG1 and IgG4 were selected for these experiments. Note, the temperature of the sample capillary was not controlled independently of the atmosphericpressure interface for the post-CAPTR activation experiments.

Figure 6a shows apparent $^{DT}\Omega_{N_2}$ distributions of $^{N}26 \rightarrow 26^*$, $^{N}26 \rightarrow 21^*$, and $^{N}26 \rightarrow 12^*$ ions of IgG1 at selected mobility cell injection voltages; corresponding distributions for IgG4 are shown in Figure S18. $\widetilde{\Omega}_{N_2}$ values of IgG1 and IgG4 $^{\rm N}26 \rightarrow C^*$ ions are shown in Figure 6b at all post-CAPTR activation voltages tested. IgG1 and IgG4 $^{\rm N}26 \rightarrow C^*$ ions exhibited very similar trends. Notably, ions of lower C exhibited a collapse in Ω with increasing injection voltage, whereas ions of intermediate C exhibited an initial collapse, and then expanded in Ω at higher injection voltages. Ions of highest C did not exhibit any evidence for collapse prior to expanding in Ω with increasing injection voltage. As discussed in the Introduction, IgGs are hypothesized to undergo significant collapse upon transition to the gas phase. ^{21–24} The lowest-C ions in these experiments exhibited evidence for collapse following activation, consistent with annealing to even more compact structures. For comparison, previous work investigating charge-state dependent activation of protein complexes with and without internal cavities showed that ions of lower charge with internal cavities accessed compact conformations at low activation voltages prior to undergoing unfolding at higher voltages.⁵³ We hypothesize that lower-C ions anneal to form more compact structures that have stronger noncovalent interactions than those present prior to annealing. In contrast, we hypothesize that higher-C ions anneal to form more extended structures that have less Coulombic repulsion, likely at the expense of other noncovalent interactions. The post-CAPTR activation results for native-like IgGs ions remain flexible and exhibit behavior that qualitatively resembles charge-reduced complexes with internal cavities.

Figure 7 shows similarity scores calculated for apparent Ω distributions of the $^{\rm N}26 \rightarrow C^*$ ions of IgG1 and IgG4 at selected post-CAPTR activation voltages. These results show that

many combinations of C and activation voltage yielded similar apparent Ω distributions for IgG1 and IgG4, notably when the values of C and the activation voltage were both large. However, other combinations yield very different apparent Ω distributions. For example, data for the $^{N}26\rightarrow C^{*}$ ions, where C=13 to 18, acquired using a post-CAPTR activation of 35 V yielded similarity scores near 0.4. Those scores are amongst the lowest found in this study (Figures 4, 5, and 7) and demonstrate that post-CAPTR activation can also provide compelling evidence that these two samples are different.

Conclusions

This study used CAPTR, pre- and post-CAPTR activation, and IM-MS (Figure 1) to characterize and compare samples of IgG1 and IgG4 from human myeloma. Consistent with previous studies, 16,21 it was challenging to distinguish between IgG1 and IgG4 using native MS or native IM-MS alone (Figures 2a-d and Figure S4). Combining CAPTR and native MS enabled more confident charge state and mass assignments, which revealed a significant mass difference between the two antibodies (Figure 2e-h). Combining CAPTR and denaturing MS, revealed intrasample heterogeneity that would have otherwise gone undetected (Figure S5D). Combining CAPTR and IM-MS reveals that for ions from native-like conditions (Figure 3), the initial ions and their charge-reduced products all have similar Ω values. For ions from denaturing conditions, each consecutive CAPTR event results in a charge-reduced product that has a smaller Ω value, but values for all products were significantly larger than those for all CAPTR products of ions from native-like conditions. In general, these trends suggest that native-like IgGs ions share many properties with other less flexible, native-like protein ions of high mass, e.g. charge density has a similar influence on gas-phase structure. 28,30,48

These samples were also analyzed using pre-CAPTR or post-CAPTR activation. With increasing pre-CAPTR activation, the Ω distributions for all ions tended to shift to larger values, increase in width, and exhibit more multimodal character. With decreasing C, the apparent Ω distributions tended to shift to smaller values, decrease in width, and exhibit more unimodal character. These trends are generally consistent with results from pre-CAPTR activation of other native-like ions of proteins. ^{28,48} With increasing post-CAPTR activation, the changes in the Ω distributions depended on the number of CAPTR events. Products with the lowest charge state exhibited a collapse in Ω with increasing injection voltage, products with the intermediate charge state exhibited an initial collapse, and then expanded in Ω at higher injection voltages, and products with the highest charge state only expanded in Ω with increasing injection voltage. This relationship between charge state and the effect of activation qualitatively resembles that reported based on CIU of charge-reduced complexes with internal cavities. 53 This suggests the IgGs ions did not fully collapse during transfer to the gas-phase. Similarity scoring was used to quantitively compare Ω distributions determined from matched experiments analyzing samples of the two antibodies, which aided in identifying experiments that maximized sample differentiation. Relative to workflows using energy-dependent IM without charge-state manipulation (Figure 5), pre-CAPTR activation (Figure 4) and post-CAPTR activation (Figure 7) both enhanced the differentiation of these antibodies by IM. In sum, CAPTR enhanced many aspects of our ability to characterize and differentiate these antibody samples. We suggest that researchers consider incorporating CAPTR into their workflows for characterizing biotherapeutics.

Supporting Information. Additional description of data analysis procedures and similarity score calculations, as well as figures of additional experimental results.

Acknowledgements

This work was supported by the National Science Foundation through awards 1807382 and 2203513 from the Division of Chemistry, with partial co-funding from the Division of Molecular and Cellular Biosciences.

References

- (1) Urquhart, L. Top Companies and Drugs by Sales in 2021. Nat. Rev. Drug Discov. 2022, 21
 (4), 251–251. https://doi.org/10.1038/d41573-022-00047-9.
- (2) Kaplon, H.; Crescioli, S.; Chenoweth, A.; Visweswaraiah, J.; Reichert, J. M. Antibodies to Watch in 2023. *mAbs* 2023, *15* (1), 2153410.
 https://doi.org/10.1080/19420862.2022.2153410.
- (3) Beck, A.; Sanglier-Cianférani, S.; Van Dorsselaer, A. Biosimilar, Biobetter, and Next Generation Antibody Characterization by Mass Spectrometry. *Anal. Chem.* **2012**, *84* (11), 4637–4646. https://doi.org/10.1021/ac3002885.
- (4) Vidarsson, G.; Dekkers, G.; Rispens, T. IgG Subclasses and Allotypes: From Structure to Effector Functions. Front. Immunol. 2014, 5, 520. https://doi.org/10.3389/fimmu.2014.00520.
- (5) Roux, K. H.; Strelets, L.; Michaelsen, T. E. Flexibility of Human IgG Subclasses. *J. Immunol.* **1997**, *159* (7), 3372–3382.
- (6) Boune, S.; Hu, P.; Epstein, A. L.; Khawli, L. A. Principles of N-Linked Glycosylation Variations of IgG-Based Therapeutics: Pharmacokinetic and Functional Considerations. *Antibodies* 2020, 9 (2), 22. https://doi.org/10.3390/antib9020022.
- (7) Harris, L. J.; Larson, S. B.; Hasel, K. W.; McPherson, A. Refined Structure of an Intact IgG2a Monoclonal Antibody. *Biochemistry* 1997, 36 (7), 1581–1597. https://doi.org/10.1021/bi962514+.
- (8) Saphire, E. O.; Parren, P. W. H. I.; Pantophlet, R.; Zwick, M. B.; Morris, G. M.; Rudd, P. M.; Dwek, R. A.; Stanfield, R. L.; Burton, D. R.; Wilson, I. A. Crystal Structure of a

- Neutralizing Human IgG Against HIV-1: A Template for Vaccine Design. *Science* **2001**, 293 (5532), 1155–1159. https://doi.org/10.1126/science.1061692.
- (9) Scapin, G.; Yang, X.; Prosise, W. W.; McCoy, M.; Reichert, P.; Johnston, J. M.; Kashi, R. S.; Strickland, C. Structure of Full-Length Human Anti-PD1 Therapeutic IgG4 Antibody Pembrolizumab. *Nat. Struct. Mol. Biol.* 2015, 22 (12), 953–958. https://doi.org/10.1038/nsmb.3129.
- (10) Xu, Y.; Wang, D.; Mason, B.; Rossomando, T.; Li, N.; Liu, D.; Cheung, J. K.; Xu, W.; Raghava, S.; Katiyar, A.; Nowak, C.; Xiang, T.; Dong, D. D.; Sun, J.; Beck, A.; Liu, H. Structure, Heterogeneity and Developability Assessment of Therapeutic Antibodies. *mAbs* **2019**, *11* (2), 239–264. https://doi.org/10.1080/19420862.2018.1553476.
- (11) Barth, M.; Schmidt, C. Native Mass Spectrometry—A Valuable Tool in Structural Biology. *J. Mass Spectrom.* **2020**, *55* (10). https://doi.org/10.1002/jms.4578.
- (12) Tamara, S.; den Boer, M. A.; Heck, A. J. R. High-Resolution Native Mass Spectrometry. *Chem. Rev.* **2022**, *122* (8), 7269–7326. https://doi.org/10.1021/acs.chemrev.1c00212.
- (13) Westphall, M. S.; Lee, K. W.; Salome, A. Z.; Lodge, J. M.; Grant, T.; Coon, J. J. Three-Dimensional Structure Determination of Protein Complexes Using Matrix-Landing Mass Spectrometry. *Nat. Commun.* **2022**, *13* (1), 2276. https://doi.org/10.1038/s41467-022-29964-4.
- (14) Esser, T. K.; Böhning, J.; Fremdling, P.; Agasid, M. T.; Costin, A.; Fort, K.; Konijnenberg, A.; Gilbert, J. D.; Bahm, A.; Makarov, A.; Robinson, C. V.; Benesch, J. L. P.; Baker, L.; Bharat, T. A. M.; Gault, J.; Rauschenbach, S. Mass-Selective and Ice-Free Electron Cryomicroscopy Protein Sample Preparation via Native Electrospray Ion-Beam Deposition. *PNAS Nexus* 2022, 1 (4), pgac153. https://doi.org/10.1093/pnasnexus/pgac153.

- (15) Deslignière, E.; Ollivier, S.; Ehkirch, A.; Martelet, A.; Ropartz, D.; Lechat, N.; Hernandez-Alba, O.; Menet, J.-M.; Clavier, S.; Rogniaux, H.; Genet, B.; Cianférani, S. Combination of IM-Based Approaches to Unravel the Coexistence of Two Conformers on a Therapeutic Multispecific mAb. *Anal. Chem.* 2022, 94 (22), 7981–7989.
 https://doi.org/10.1021/acs.analchem.2c00928.
- (16) Tian, Y.; Han, L.; Buckner, A. C.; Ruotolo, B. T. Collision Induced Unfolding of Intact Antibodies: Rapid Characterization of Disulfide Bonding Patterns, Glycosylation, and Structures. *Anal. Chem.* 2015, 87 (22), 11509–11515. https://doi.org/10.1021/acs.analchem.5b03291.
- (17) Deslignière, E.; Botzanowski, T.; Diemer, H.; Cooper-Shepherd, D. A.; Wagner-Rousset, E.; Colas, O.; Béchade, G.; Giles, K.; Hernandez-Alba, O.; Beck, A.; Cianférani, S. High-Resolution IMS–MS to Assign Additional Disulfide Bridge Pairing in Complementarity-Determining Regions of an IgG4 Monoclonal Antibody. *J. Am. Soc. Mass Spectrom.* 2021, 32 (10), 2505–2512. https://doi.org/10.1021/jasms.1c00151.
- (18) Upton, R.; Migas, L. G.; Pacholarz, K. J.; Beniston, R. G.; Estdale, S.; Firth, D.; Barran, P. E. Hybrid Mass Spectrometry Methods Reveal Lot-to-Lot Differences and Delineate the Effects of Glycosylation on the Tertiary Structure of Herceptin®. *Chem. Sci.* 2019, 10 (9), 2811–2820. https://doi.org/10.1039/C8SC05029E.
- (19) Marcoux, J.; Champion, T.; Colas, O.; Wagner-Rousset, E.; Corvaïa, N.; Van Dorsselaer, A.; Beck, A.; Cianférani, S. Native Mass Spectrometry and Ion Mobility Characterization of Trastuzumab Emtansine, a Lysine-Linked Antibody Drug Conjugate: Native MS and IM-MS for Trastuzumab Emtansine Analysis. *Protein Sci.* 2015, 24 (8), 1210–1223. https://doi.org/10.1002/pro.2666.

- (20) Pacholarz, K. J.; Barran, P. E. Use of a Charge Reducing Agent to Enable Intact Mass Analysis of Cysteine-Linked Antibody-Drug-Conjugates by Native Mass Spectrometry. *EuPA Open Proteomics* **2016**, *11*, 23–27. https://doi.org/10.1016/j.euprot.2016.02.004.
- (21) Pacholarz, K. J.; Porrini, M.; Garlish, R. A.; Burnley, R. J.; Taylor, R. J.; Henry, A. J.; Barran, P. E. Dynamics of Intact Immunoglobulin G Explored by Drift-Tube Ion-Mobility Mass Spectrometry and Molecular Modeling. *Angew. Chem. Int. Ed.* 2014, *53* (30), 7765–7769. https://doi.org/10.1002/anie.201402863.
- (22) Campuzano, I. D. G.; Larriba, C.; Bagal, D.; Schnier, P. D. Ion Mobility and Mass Spectrometry Measurements of the Humanized IgGk NIST Monoclonal Antibody. In *ACS Symposium Series*; Schiel, J. E., Davis, D. L., Borisov, O. V., Eds.; American Chemical Society: Washington, DC, 2015; Vol. 1202, pp 75–112. https://doi.org/10.1021/bk-2015-1202.ch004.
- (23) Hansen, K.; Lau, A. M.; Giles, K.; McDonnell, J. M.; Struwe, W. B.; Sutton, B. J.; Politis, A. A Mass-Spectrometry-Based Modelling Workflow for Accurate Prediction of IgG Antibody Conformations in the Gas Phase. *Angew. Chem. Int. Ed.* 2018, 57 (52), 17194–17199. https://doi.org/10.1002/anie.201812018.
- (24) Devine, P. W. A.; Fisher, H. C.; Calabrese, A. N.; Whelan, F.; Higazi, D. R.; Potts, J. R.; Lowe, D. C.; Radford, S. E.; Ashcroft, A. E. Investigating the Structural Compaction of Biomolecules Upon Transition to the Gas-Phase Using ESI-TWIMS-MS. *J. Am. Soc. Mass Spectrom.* 2017, 28 (9), 1855–1862. https://doi.org/10.1007/s13361-017-1689-9.
- (25) Deslignière, E.; Ollivier, S.; Beck, A.; Ropartz, D.; Rogniaux, H.; Cianférani, S. Benefits and Limitations of High-Resolution Cyclic IM-MS for Conformational Characterization of

- Native Therapeutic Monoclonal Antibodies. *Anal. Chem.* **2023**, acs.analchem.2c05265. https://doi.org/10.1021/acs.analchem.2c05265.
- (26) Wang, G.; Cole, R. B. Solution, Gas-Phase, and Instrumental Parameter Influences on Charge-State Distributions in Electrospray Ionization Mass Spectrometry. In *Electrospray* ionization mass spectrometry: fundamentals, instrumentation, and applications; Cole, R. B., Ed.; Wiley: New York, 1997; pp 137–174.
- (27) Allen, S. J.; Schwartz, A. M.; Bush, M. F. Effects of Polarity on the Structures and Charge States of Native-Like Proteins and Protein Complexes in the Gas Phase. *Anal. Chem.* **2013**, 85 (24), 12055–12061. https://doi.org/10.1021/ac403139d.
- (28) Gadzuk-Shea, M. M.; Bush, M. F. Effects of Charge State on the Structures of Serum Albumin Ions in the Gas Phase: Insights from Cation-to-Anion Proton-Transfer Reactions, Ion Mobility, and Mass Spectrometry. J. Phys. Chem. B 2018, 122 (43), 9947–9955. https://doi.org/10.1021/acs.jpcb.8b08427.
- (29) Han, Z.; Chen, L. C. High-Pressure nanoESI of Highly Conductive Volatile and Non-Volatile Buffer Solutions from a Large Taylor Cone: Effect of Spray Current on Charge State Distribution. *Int. J. Mass Spectrom.* 2022, 476, 116845.
 https://doi.org/10.1016/j.ijms.2022.116845.
- (30) Gozzo, T. A.; Bush, M. F. Effects of Charge on Protein Ion Structure: Lessons from Cation-to-Anion Proton-Transfer Reactions. *Mass Spectrom. Rev.* **2023**, DOI: 10.1002/mas.21847.
- (31) Stephenson, J. L.; McLuckey, S. A. Ion/Ion Proton Transfer Reactions for Protein Mixture Analysis. *Anal. Chem.* **1996**, *68* (22), 4026–4032. https://doi.org/10.1021/ac9605657.
- (32) Abzalimov, R. R.; Kaltashov, I. A. Electrospray Ionization Mass Spectrometry of Highly Heterogeneous Protein Systems: Protein Ion Charge State Assignment via Incomplete

- Charge Reduction. *Anal. Chem.* **2010**, *82* (18), 7523–7526. https://doi.org/10.1021/ac101848z.
- (33) Laszlo, K. J.; Bush, M. F. Analysis of Native-Like Proteins and Protein Complexes Using Cation to Anion Proton Transfer Reactions (CAPTR). *J. Am. Soc. Mass Spectrom.* **2015**, *26* (12), 2152–2161. https://doi.org/10.1007/s13361-015-1245-4.
- (34) Huguet, R.; Mullen, C.; Srzentić, K.; Greer, J. B.; Fellers, R. T.; Zabrouskov, V.; Syka, J. E. P.; Kelleher, N. L.; Fornelli, L. Proton Transfer Charge Reduction Enables High-Throughput Top-Down Analysis of Large Proteoforms. *Anal. Chem.* 2019, 91 (24), 15732–15739. https://doi.org/10.1021/acs.analchem.9b03925.
- (35) McLuckey, S. A.; Stephenson, J. L. Ion/Ion Chemistry of High-Mass Multiply Charged Ions. *Mass Spectrom. Rev.* 1998, 17 (6), 369–407. https://doi.org/10.1002/(SICI)1098-2787(1998)17:6<369::AID-MAS1>3.0.CO;2-J.
- (36) Laszlo, K. J.; Buckner, J. H.; Munger, E. B.; Bush, M. F. Native-Like and Denatured Cytochrome c Ions Yield Cation-to-Anion Proton Transfer Reaction Products with Similar Collision Cross-Sections. *J. Am. Soc. Mass Spectrom.* 2017, 28 (7), 1382–1391. https://doi.org/10.1007/s13361-017-1620-4.
- (37) Laszlo, K. J.; Munger, E. B.; Bush, M. F. Effects of Solution Structure on the Folding of Lysozyme Ions in the Gas Phase. *J. Phys. Chem. B* **2017**, *121* (13), 2759–2766. https://doi.org/10.1021/acs.jpcb.7b00783.
- (38) Laszlo, K. J.; Munger, E. B.; Bush, M. F. Folding of Protein Ions in the Gas Phase after Cation-to-Anion Proton-Transfer Reactions. *J. Am. Chem. Soc.* **2016**, *138* (30), 9581–9588. https://doi.org/10.1021/jacs.6b04282.

- (39) Hong, S.; Bush, M. F. Collision-Induced Unfolding Is Sensitive to the Polarity of Proteins and Protein Complexes. *J. Am. Soc. Mass Spectrom.* **2019**, *30* (11), 2430–2437. https://doi.org/10.1007/s13361-019-02326-z.
- (40) Lin, J. Divergence Measures Based on the Shannon Entropy. *IEEE Trans. Inf. Theory* **1991**, 37 (1), 145–151. https://doi.org/10.1109/18.61115.
- (41) Endres, D. M.; Schindelin, J. E. A New Metric for Probability Distributions. *IEEE Trans. Inf. Theory* **2003**, *49* (7), 1858–1860. https://doi.org/10.1109/TIT.2003.813506.
- (42) Österreicher, F.; Vajda, I. A New Class of Metric Divergences on Probability Spaces and Its Applicability in Statistics. *Ann. Inst. Stat. Math.* **2003**, *55* (3), 639–653. https://doi.org/10.1007/BF02517812.
- (43) Williams, J. P.; Brown, J. M.; Campuzano, I.; Sadler, P. J. Identifying Drug Metallation Sites on Peptides Using Electron Transfer Dissociation (ETD), Collision Induced Dissociation (CID) and Ion Mobility-Mass Spectrometry (IM-MS). *Chem. Commun.* 2010, 46 (30), 5458. https://doi.org/10.1039/c0cc00358a.
- (44) Allen, S. J.; Giles, K.; Gilbert, T.; Bush, M. F. Ion Mobility Mass Spectrometry of Peptide, Protein, and Protein Complex Ions Using a Radio-Frequency Confining Drift Cell. *Analyst* 2016, 141 (3), 884–891. https://doi.org/10.1039/C5AN02107C.
- (45) Davidson, K. L.; Oberreit, D. R.; Hogan, C. J.; Bush, M. F. Nonspecific Aggregation in Native Electrokinetic Nanoelectrospray Ionization. *Int. J. Mass Spectrom.* **2017**, *420*, 35–42. https://doi.org/10.1016/j.ijms.2016.09.013.
- (46) Thompson, N. J.; Rosati, S.; Heck, A. J. R. Performing Native Mass Spectrometry Analysis on Therapeutic Antibodies. *Methods* 2014, 65 (1), 11–17. https://doi.org/10.1016/j.ymeth.2013.05.003.

- (47) Bush, M. F.; Campuzano, I. D. G.; Robinson, C. V. Ion Mobility Mass Spectrometry of Peptide Ions: Effects of Drift Gas and Calibration Strategies. *Anal. Chem.* 2012, 84 (16), 7124–7130. https://doi.org/10.1021/ac3014498.
- (48) Laszlo, K. J.; Bush, M. F. Interpreting the Collision Cross Sections of Native-like Protein Ions: Insights from Cation-to-Anion Proton-Transfer Reactions. *Anal. Chem.* 2017, 89 (14), 7607–7614. https://doi.org/10.1021/acs.analchem.7b01474.
- (49) Sobott, F.; McCammon, M. G.; Robinson, C. V. Gas-Phase Dissociation Pathways of a Tetrameric Protein Complex. *Int. J. Mass Spectrom.* **2003**, *230* (2–3), 193–200. https://doi.org/10.1016/j.ijms.2003.09.008.
- (50) Sims, G. E.; Jun, S.-R.; Wu, G. A.; Kim, S.-H. Alignment-Free Genome Comparison with Feature Frequency Profiles (FFP) and Optimal Resolutions. *Proc. Natl. Acad. Sci.* **2009**, *106* (8), 2677–2682. https://doi.org/10.1073/pnas.0813249106.
- (51) Martins, A.; Smith, N.; Xing, E.; Aguiar, P.; Figueiredo, M. Nonextensive Information Theoretic Kernels on Measures. *J. Mach. Learn. Res.* **2009**, *10*, 935–975.
- (52) Mehri, A.; Jamaati, M.; Mehri, H. Word Ranking in a Single Document by Jensen–Shannon Divergence. *Phys. Lett. A* 2015, 379 (28–29), 1627–1632. https://doi.org/10.1016/j.physleta.2015.04.030.
- (53) Hall, Z.; Politis, A.; Bush, M. F.; Smith, L. J.; Robinson, C. V. Charge-State Dependent Compaction and Dissociation of Protein Complexes: Insights from Ion Mobility and Molecular Dynamics. *J. Am. Chem. Soc.* 2012, 134 (7), 3429–3438. https://doi.org/10.1021/ja2096859.

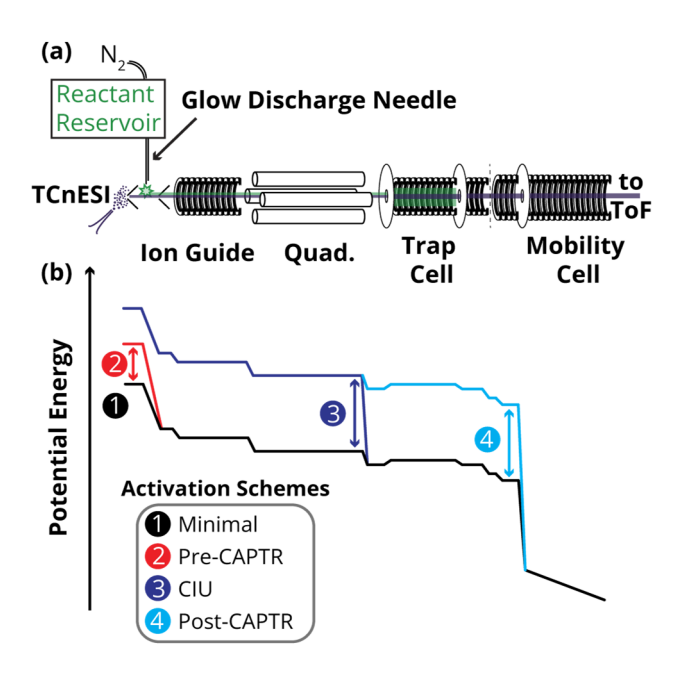


Figure 1. (a) Diagram of the modified Waters Synapt G2 HDMS with radio-frequency confining drift cell. Anions (green) are generated by glow-discharge ionization and accumulated in the trap cell. Cations (purple) are generated by nanoelectrospray ionization and transmitted through the anion population in the trap cell for CAPTR. Residual precursor and CAPTR product ions are separated by IM prior to mass analysis. (b) Representative potential-energy diagrams for cation transmission during minimal activation, pre-CAPTR activation, collision-induced unfolding (CIU), and post-CAPTR activation experiments. Figure adapted with permission from *J. Am. Chem. Soc.* **2016**, *138*, 9581–9588.³⁸ Copyright 2016 American Chemical Society.

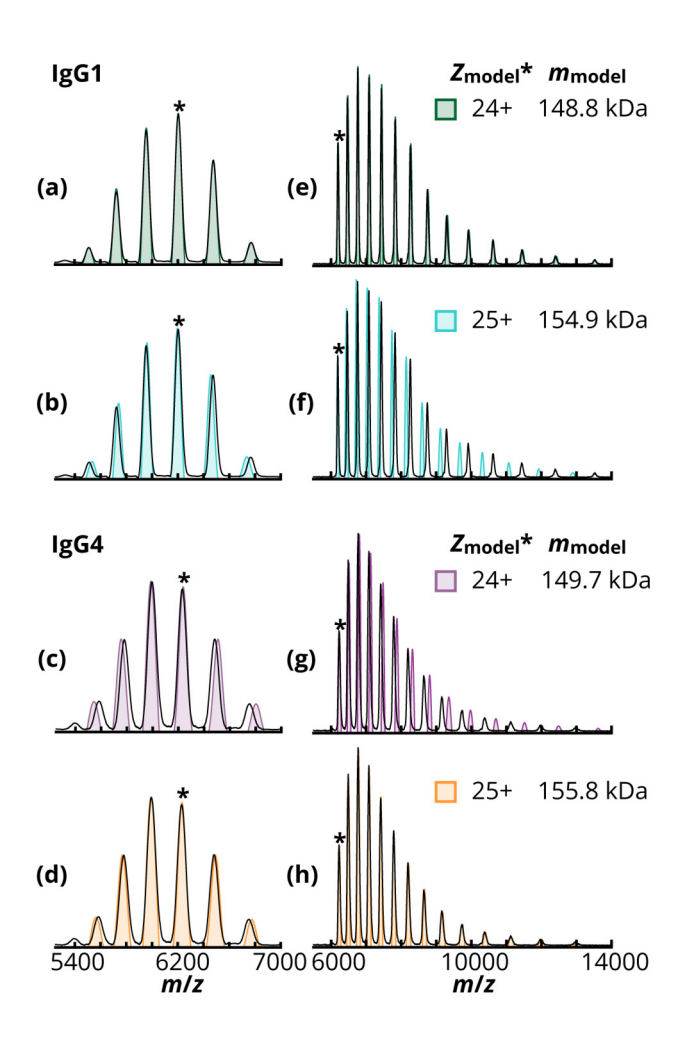


Figure 2. (a-d) The IgG1 (a, b) and IgG4 (c, d) experimental mass spectra of ions from native-like conditions (black) are overlayed with simulated mass spectra based on the charge assignment of the peaks centered near 6195 *m/z* (IgG1) and 6227 *m/z* (IgG4). Assignment of the indicated IgG1 peak as 24+ (a, green) or 25+ (b, blue) results in mass determinations of 148.8 and 154.9 kDa, respectively. Assignment of the indicated IgG4 peak as 24+ (c, purple) or 25+ (d, orange) results in mass determinations of 148.7 and 155.7 kDa, respectively. (e)-(h) show the experimental mass spectra (black) of the CAPTR products generated after quadrupole of the indicated ions; corresponding CAPTR mass spectra were simulated using the masses determined from the models of the native mass spectra.

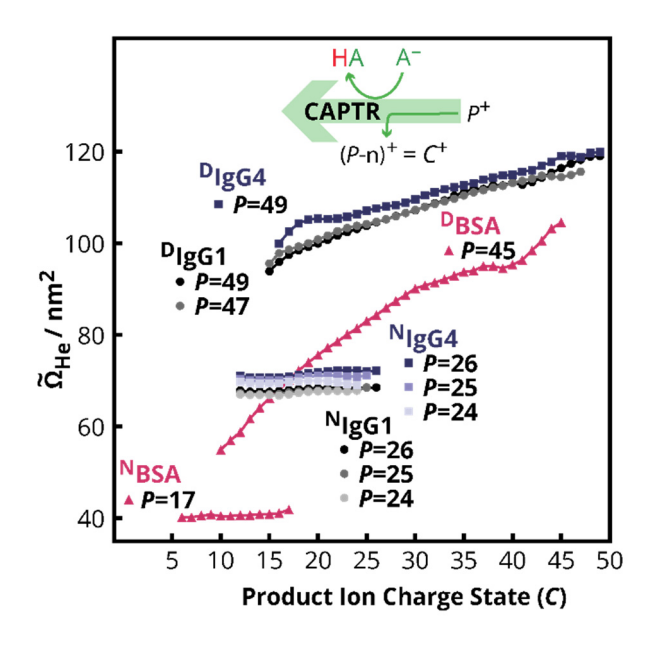


Figure 3. DT ΩHe values of IgG1, IgG4, and BSA ions produced from electrospray from native-like and denaturing solution conditions and subjected to CAPTR. Denaturing conditions used for BSA experiments were comprised of 70:30 water/methanol with 0.2% formic acid; native-like conditions were the same as those used for IgGs. Precursors 26+, 25+, and 24+ were selected for CAPTR of NIgGs, and precursors 47+ and 49+ were selected for CAPTR of DIgGs. Note that CAPTR of DIgG4 47+ ions revealed the presence of two species within the sample (Figure S4); these IM results are not shown. The 45+ and 17+ precursors were selected for CAPTR of DBSA and NBSA, respectively.

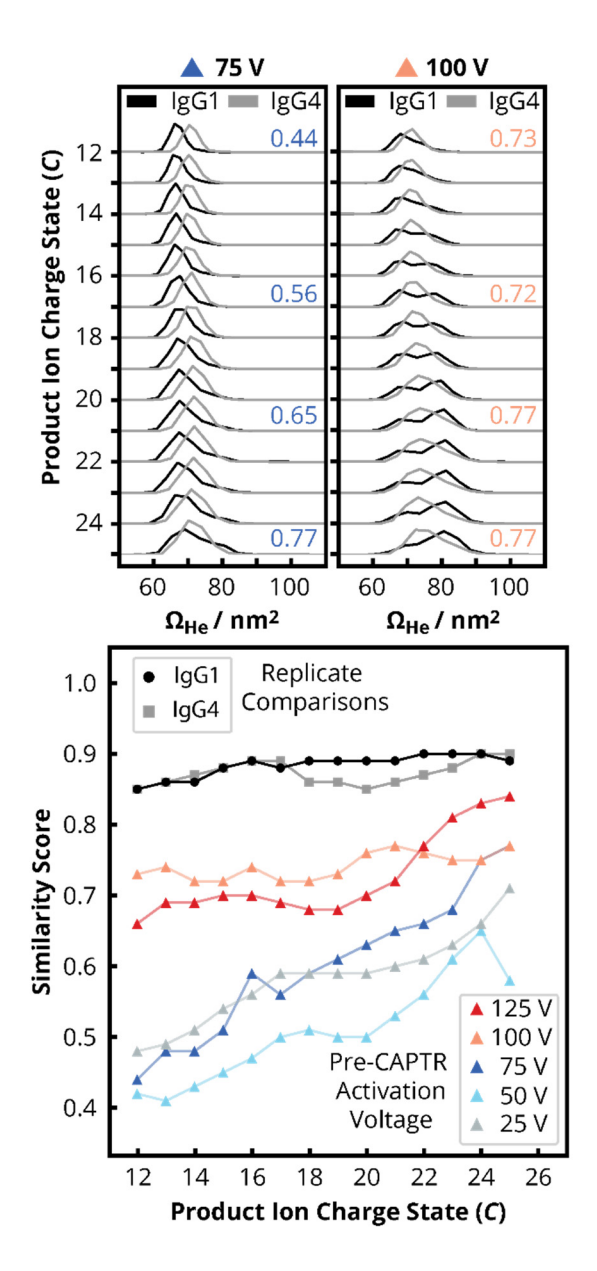


Figure 4. (Top) The apparent $^{DT}\Omega_{He}$ distributions of CAPTR products and residual precursor ions generated after activation (75 V and 100 V, pre-CAPTR activation) of 25+ precursors. Similarity scores are provided for representative distribution comparisons. (Bottom) The similarity scores for comparison of the apparent $^{DT}\Omega_{He}$ distributions of replicates of IgG1 and IgG4 $^{N}25\rightarrow C$ versus charge state (triangles) and the similarity scores for the comparison of the apparent $^{DT}\Omega_{He}$ distributions of IgG1 and IgG4 at different pre-CAPTR activation voltages versus charge state (circles). For most pre-CAPTR activation voltages, the $^{DT}\Omega_{He}$ distributions of the lower charged ions are more distinguishable (lower similarity scores) than those of their activated precursors.

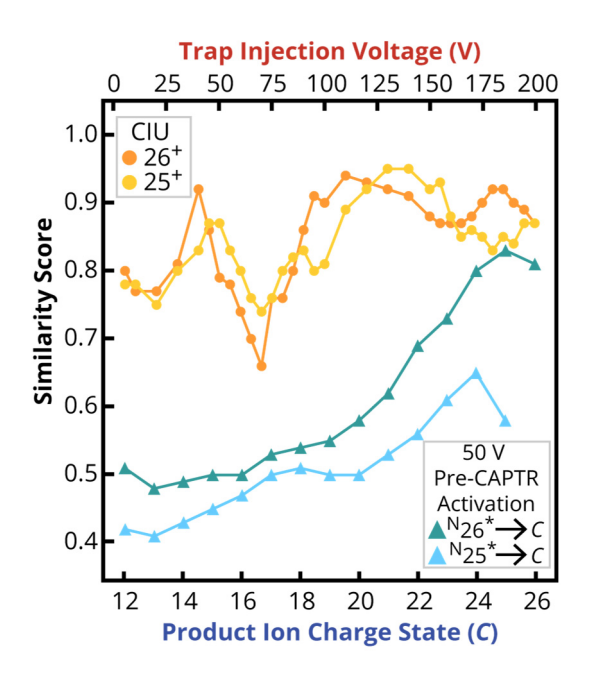


Figure 5. The similarity scores of the apparent ^{DT}Ω_{He} distributions of ^NIgG1 and ^NIgG4 CAPTR products and residual precursor (25+ and 26+) ions at 50 V pre-CAPTR activation versus charge state (cool colors, bottom axis), and the similarity scores of apparent ^{DT}Ω_{He} distributions of ^NIgG1 and ^NIgG4 precursor ions (25+ and 26+) subjected to collision-induced unfolding versus trap collision energy (warm colors, top axis). The distributions of charge-reduced products are more distinguishable (lower similarity scores) than those of the precursor ions subjected to CIU.

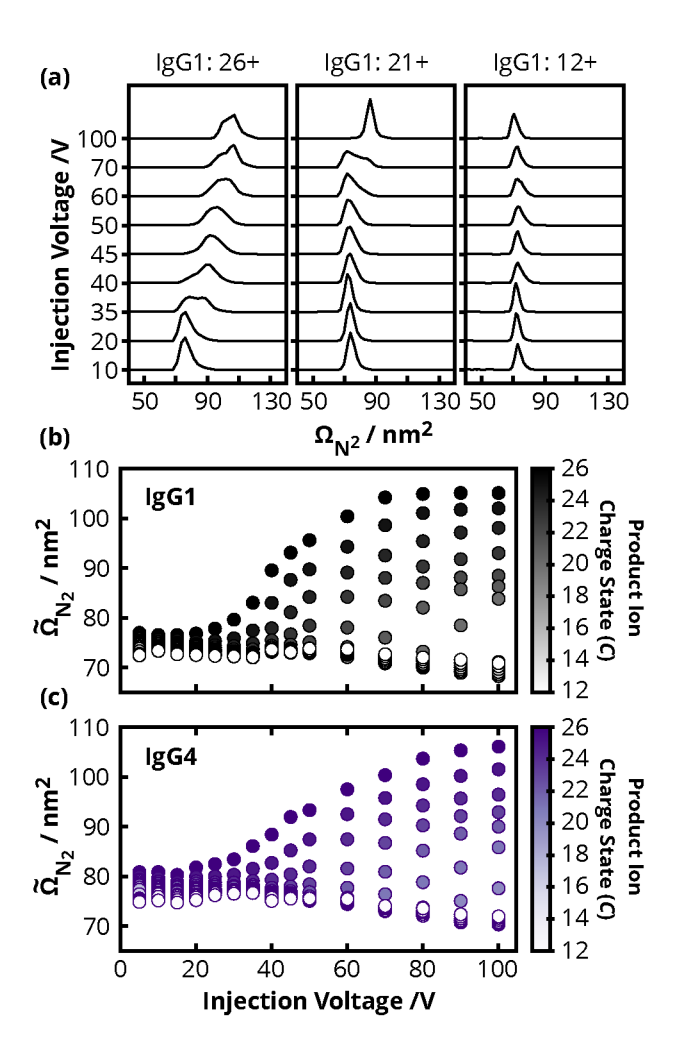


Figure 6. Post-CAPTR activation of ${}^{N}IgG1$ and ${}^{N}IgG4$. (a) Apparent $\Omega_{N_{2}}$ distributions of ${}^{N}26 \rightarrow 26^{*}$, ${}^{N}26 \rightarrow 21^{*}$, and ${}^{N}26 \rightarrow 12^{*}$ ions of IgG1 at selected mobility cell injection voltages. (b) $\widetilde{\Omega}_{N_{2}}$ values of each $IgG1 \, {}^{N}26 \rightarrow C^{*}$ ion population as a function of mobility cell injection voltage. (c) $\widetilde{\Omega}_{N_{2}}$ values of each $IgG4 \, {}^{N}26 \rightarrow C^{*}$ ion population as a function of mobility cell injection voltage.

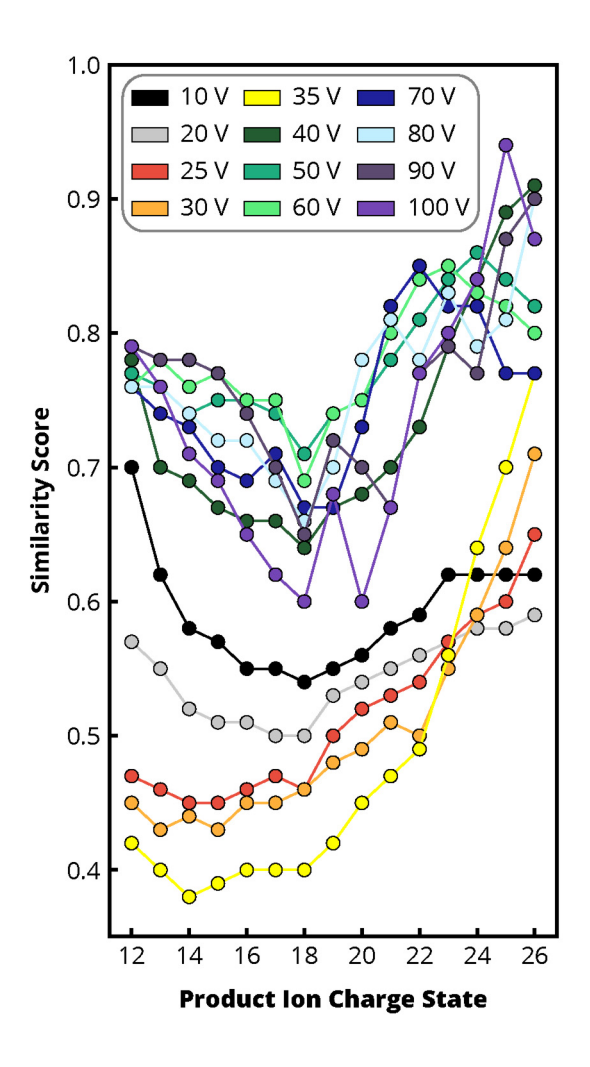


Figure 7. Similarity scores comparing the apparent Ω_{N_2} distributions of $^{N}26 \rightarrow C^*$ ions of IgG1 and IgG4 at different post-CAPTR activation voltages.

For Table of Contents

